INTERNATIONAL JOURNAL OF
RADIATION ONCOLOGY • BIOLOGY • PHYSICS
www.redjournal.org

PHYSICS CONTRIBUTION

Pencil-beam Delivery Pattern Optimization Increases Dose Rate for Stereotactic FLASH Proton Therapy

Rodrigo José Santo, MSc,[*,†,‡] Steven J.M. Habraken, PhD,[*,‡] Sebastiaan Breedveld, PhD,[*] and Mischa S. Hoogeman, PhD[*,‡]

[*]*Erasmus MC Cancer Institute, University Medical Center Rotterdam, Department of Radiotherapy, Rotterdam, The Netherlands;* [†]*Instituto Superior Técnico, Department of Physics, Universidade de Lisboa, Lisbon, Portugal; and* [‡]*Holland Proton Therapy Center, Department of Medical Physics & Informatics, Delft, The Netherlands*

Received Jan 26, 2022; Accepted for publication Aug 22, 2022

Purpose: FLASH dose rates >40 Gy/s are readily available in proton therapy (PT) with cyclotron-accelerated beams and pencil-beam scanning (PBS). The PBS delivery pattern will affect the local dose rate, as quantified by the PBS dose rate (PBS-DR), and therefore needs to be accounted for in FLASH-PT with PBS, but it is not yet clear how. Our aim was to optimize patient-specific scan patterns for stereotactic FLASH-PT of early-stage lung cancer and lung metastases, maximizing the volume irradiated with PBS-DR >40 Gy/s of the organs at risk voxels irradiated to >8 Gy (FLASH coverage).

Methods and Materials: Plans to 54 Gy/3 fractions with 3 equiangular coplanar 244 MeV proton shoot-through transmission beams for 20 patients were optimized with in-house developed software. Planning target volume-based planning with a 5 mm margin was used. Planning target volume ranged from 4.4 to 84 cc. Scan-pattern optimization was performed with a Genetic Algorithm, run in parallel for 20 independent populations (islands). Mapped crossover, inversion, swap, and shift operators were applied to achieve (local) optimality on each island, with migration between them for global optimality. The cost function was chosen to maximize the FLASH coverage per beam at >8 Gy, >40 Gy/s, and 40 nA beam current. The optimized patterns were evaluated on FLASH coverage, PBS-DR distribution, and population PBS-DR-volume histograms, compared with standard line-by-line scanning. Robustness against beam current variation was investigated.

Results: The optimized patterns have a snowflake-like structure, combined with outward swirling for larger targets. A population median FLASH coverage of 29.0% was obtained for optimized patterns compared with 6.9% for standard patterns, illustrating a significant increase in FLASH coverage for optimized patterns. For beam current variations of 5 nA, FLASH coverage varied between −6.1%-point and 2.2%-point for optimized patterns.

Conclusions: Significant improvements on the PBS-DR and, hence, on FLASH coverage and potential healthy-tissue sparing are obtained by sequential scan-pattern optimization. The optimizer is flexible and may be further fine-tuned, based on the exact conditions for FLASH.

Corresponding author: Steven J.M. Habraken, PhD;
E-mail: s.habraken@erasmusmc.nl

Disclosures: none.

Data Sharing Statement: Research data are stored in an institutional repository and will be shared upon request to the corresponding author.

Acknowledgments—We thank Daniel Tsang for initial analytical modeling and numerical experiments on scanning patterns in FLASH proton therapy with pencil-beam scanning and optimization thereof.

Supplementary material associated with this article can be found in the online version at doi:10.1016/j.ijrobp.2022.08.053.

https://doi.org/10.1016/j.ijrobp.2022.08.053

Introduction

Since the seminal article by Favaudon et al was published in 2014,[1] the FLASH effect has generated a lot of interest in the broader radiation therapy community. It has been repeatedly observed in preclinical experiments for high-dose (>8 Gy) and ultrahigh dose-rate (UHDR, >40 Gy/s) irradiation and amounts to a significant reduction of the radiosensitivity of healthy tissue while maintaining tumor control. Although the fact that radiosensitivity may be substantially lower at UHDRs was first discovered in the late 1950s and 1960s,[2,3] FLASH as a differential effect between tumor and healthy tissue provides a new and fundamentally different approach to further increase the therapeutic bandwidth of radiation therapy. The mechanisms behind are still not fully unraveled, but nonmutually exclusive explanations described in literature focus on the role of oxygen,[4] other aspects of radiochemistry, and the radiosensitivity of the immune system.[5]

FLASH was first demonstrated and has been most extensively studied in radiobiological experiments with MeV electron beams.[6,7] A first patient has been successfully treated with FLASH electron beam therapy in Lausanne in 2019.[8] FLASH compatible dose rates are, however, readily available in high-energy (up to 250 MeV) proton beams. Recent research has demonstrated the FLASH effect also exist in such beams.[9-14] Patient accrual of a first in-human clinical trial on FLASH proton therapy (FLASH-PT) of bone metastases in extremity has been completed recently.[15] Hence, FLASH proton therapy may be feasible with current commercially available cyclotron-accelerated therapeutic proton beams. Although 4.5 to 10 MeV electron beams are limited to treatments up to a few centimeters depth, FLASH proton therapy may be particularly suited for deep-seated targets.

The overall highest dose rate is achieved at the maximum cyclotron energy of 250 MeV. Such beams may shoot-through the patient and are referred to as transmission beams (no Bragg peak inside the patient). Their use may be advantageous for some clinical applications[16-18] as they mitigate proton stopping power prediction (range) uncertainty and maintain a sharp lateral penumbra at all depths. The lateral extent of even the smallest tumors cannot be adequately covered with a single pencil beam. Therefore, the 250 MeV pristine FLASH beam needs to be combined with lateral pencil-beam scanning (PBS), leading to a complex and spatially varying time structure in the dose delivery. To report FLASH dose-rate and optimize it, various metrics and optimization methods have been proposed.[19-22]

In a recent article, Folkerts et al[22] proposed the pencil-beam scanning dose rate (PBS-DR). Assuming that FLASH is a local effect and that the total irradiation time is a critical FLASH parameter, this metric is voxel-based and defined as dose delivered per fraction to a given voxel, divided by the effective irradiation time, defined based on a fixed dose threshold. The effective irradiation time starts when the accumulated dose reaches the threshold and stops when it has increased to the total dose minus that threshold. As a local FLASH effect depends on the spatiotemporal structure of dose delivery, it can, in part, be optimized through scan-pattern optimization.

In this article, we describe and evaluate a novel sequential optimization of the scan pattern in stereotactic FLASH-PT with PBS for early-stage lung cancer and lung metastases, focusing on single-beam per fraction treatments to enable delivery within FLASH dose and dose-rate thresholds (see below). We present a scan-pattern optimizer, based on a (stochastic) genetic algorithm, configured to optimize the order in which a predefined set of pencil beams with preoptimized weights is delivered. This sequential scan-pattern optimization is tuned to optimize the FLASH coverage per beam in treatment delivery (ie, the volume of healthy tissue irradiated within strict FLASH conditions). The optimized scan patterns are evaluated on the FLASH coverage, PBS-DR distribution, and population PBS-DR-volume histograms, compared with standard nonoptimized line-by-line scanning.

Methods and Materials

Patient data

A cohort of 20 patients with peripheral lung lesions, clinically treated in 3 fractions with photons on a CyberKnife was used, including both lung metastases and early-stage primary lung cancer cases. Only patients treated for a single lesion in one treatment plan were included. Clinical gross tumor volume (GTV; GTV = clinical target volume [CTV] for these patients) delineations were available, and a fixed 5 mm margin was applied to the planning target volume (PTV). The median PTV was 8.7 cc (range, 4.4-84 cc).

Treatment planning

Proton therapy treatment planning was implemented in Erasmus-iCycle[23], our in-house developed software for multicriteria optimization of radiation therapy treatment plans. It uses the Astroid proton dose engine[24] and the beam model for the clinical HollandPTC Varian ProBeam setup, commissioned previously.[25] Equiangular coplanar arrangements of 3 244 MeV proton beams, the highest energy available in the current clinical beam model, at gantry angles of 40, 160, and 280 degrees were used. These pencil beams have a width of (1 standard deviation) of 3.31 mm at the snout and shoot through the patient in stereotactic lung treatments due to their 35.8 cm range in water. Beam directions were inverted when necessary to have the shortest path from the entrance to the PTV. The common regimen of 54 Gy in 3 fractions[26] was used. For the physical dose distribution to comply with clinical guidelines, constraints were put on (1) the minimum dose to CTV ($\geq$100% D_{pres}) and PTV ($\geq$98% D_{pres}) and (2) the maximum dose to critical serial OARs, ie, esophagus ($\leq$31.5 Gy), spinal cord

(≤21.6 Gy), trachea (≤36 Gy), and ipsilateral bronchus (≤38.1 Gy). Prioritized objectives were used on maximum dose to (1) the PTV (≤124% D_{pres}), (2) the CTV (≤124% D_{pres}), (3) 3 mm (≤62% D_{pres}), and 6 mm (≤31% D_{pres}) shells around the PTV (respectively ≤62% D_{pres} and ≤31% D_{pres}), and (4) to all OARs and other (nontarget) healthy tissue. All plans were evaluated based on our clinical protocol, which, besides the D_{max} constraints listed above, also requires V_{13Gy} ≤31% for healthy lung. To enable single-beam per fraction delivery, a single field (beam) uniform dose approach was used with $D_{95\%,PTV}$ = 100% D_{pres} per beam. Initial pencil-beam placement was done on a 5 mm grid. Pencil-beam reduction,[27] iteratively removing low-weighted pencil beams and reoptimizing the remaining pencil-beam weights, was used to reduce delivery time. The median number of pencil beams was 51 (full range, 26-171) per beam direction. For more details with regards to treatment planning, we refer to XXX et al.[28] For a technologically feasible and relatively modest nozzle current of 40 nA, the median estimated pencil-beam delivery time for all plans was 22.3 ms (full range, 0.002-66.8 ms, with 95% of values from 20.3-21.1 ms) and 1.6% of pencil beams had estimated delivery time below 1 ms. Without pencil-beam switching times (see below), the median estimated fraction delivery time was 914 ms (full range, 622-3876 ms).

FLASH modeling

As it is not clear yet how to combine the FLASH effect for multiple beams delivered in consecutive fractions or within the same fraction, the dose rate and, therefore, FLASH is evaluated for each treatment beam separately. For single-beam per fraction delivery, the FLASH effect was modeled with a simple binary model: all voxels excluding the GTV irradiated to a beam dose >8 Gy at PBS-DR >40 Gy/s are considered FLASH compatible. The scan patterns were evaluated in terms of FLASH coverage, defined as the volume (percentage) of healthy tissue irradiated within strict FLASH conditions. The sensitivity of the FLASH coverage on beam current was assessed for the optimized and standard (non-optimized) line-by-line patterns. To this end, the FLASH coverage was recalculated for a beam current ranging from 20 to 60 nA in steps of 5 nA.

Scan-pattern optimization

Figure 1 shows at what stage in the treatment planning process scan-pattern optimization (SPO) has been implemented. It is performed sequentially after the optimization of pencil-beam positions and weights, modifying only the order in which the optimized pencil beams are delivered. In this way, SPO was implemented without any compromise or trade-off on plan quality in terms of (nominal) absorbed dose.

SPO is a highly nonlinear, nondifferentiable combinatorial problem. Therefore, a genetic algorithm (GA) was used. GAs constitute a subclass of evolutionary algorithms and have been studied extensively in mathematical literature on traveling salesmen[29] and other combinatorial problems.[30] Scan patterns are encoded by the order in which the pencil beams are delivered and their evolution through the algorithm is guided by the FLASH coverage per beam as a global evaluation metric. To promote regularity of the pattern and minimize the total distance traversed in the plane transverse to the beam direction, the average distance between subsequent pencil beams was added as an additional cost function. It was normalized to the 5-mm pencil beam grid spacing and weighted with a factor of 0.005, relative to the (dimensionless) FLASH coverage, which was sufficient to steer the GA while not compromising FLASH coverage.

A schematic overview of the GA is shown in Figure 2. The GA was implemented in Python 3.7.9, with source code in the SimpleGP library.[31] The SPO was performed on a computer cluster with a 20-core 2.50 GHz Intel Xeon processor, 50 GB of RAM and 4 cores per node and 2 nodes allocated for each job. The GA takes the beam current at the nozzle, the pencil-beam weights, and the dose deposition matrix, which characterizes the dose from each pencil beam to each voxel, as input. Pencil-beam switching times (ie, dead time between the delivery of consecutive pencil beams), which are on the order of a few tenths of milliseconds, were neglected as they contribute a fixed but comparably small portion of the beam delivery time and, therefore, have minor effect only on the pattern optimization. Each

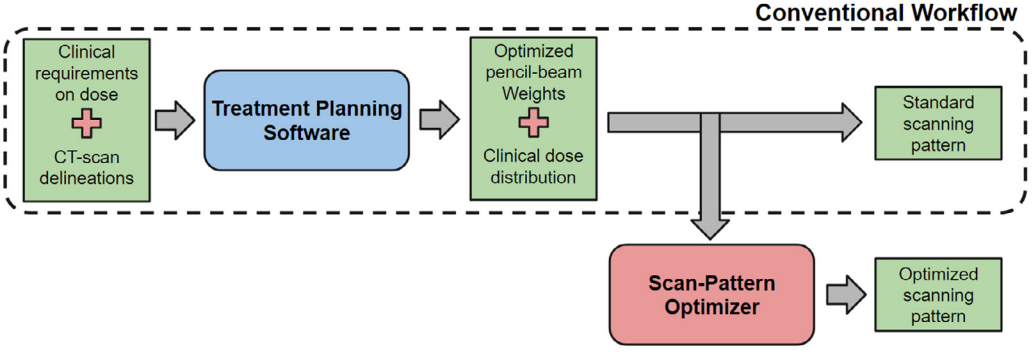

Fig. 1. Integration of scan-pattern optimization (SPO) within the conventional clinical workflow.

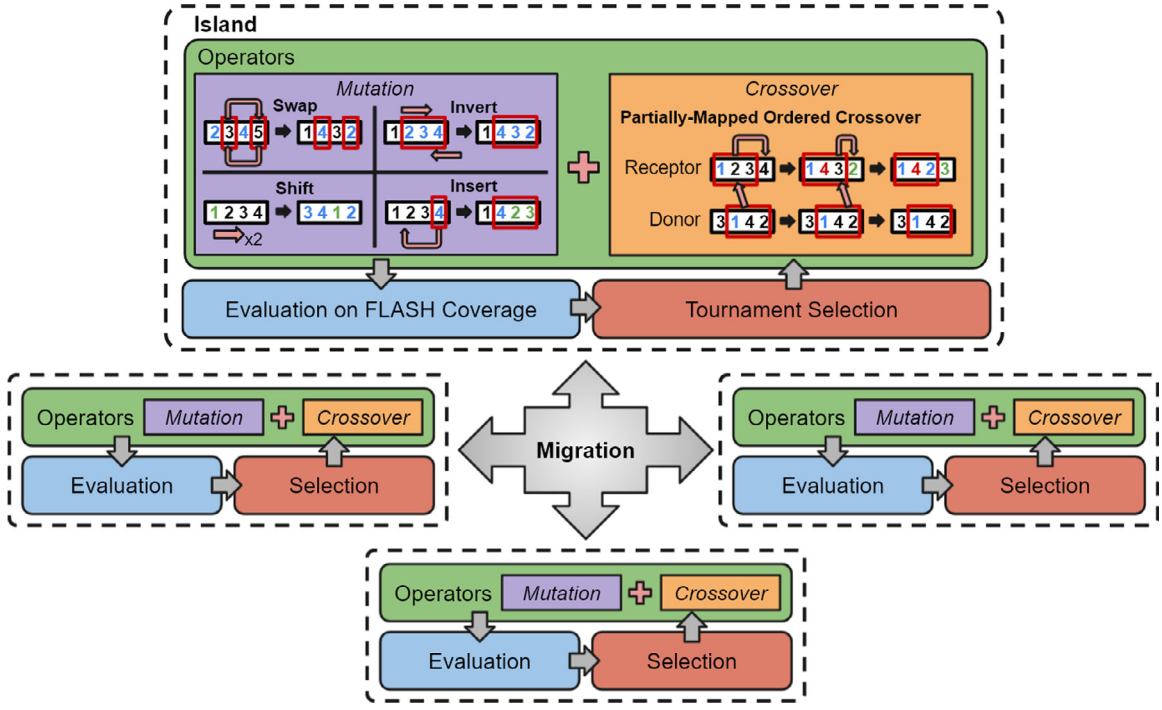

Fig. 2. Structure of the island model genetic algorithm (IMGA), illustrating how different island evolve independently with the proposed operators, only communicating between them through migration.

individual pattern of a population of 50 times the number of pencil beams is initialized to a random scan pattern. Mutation was implemented through swap, invert, shift and insert operations, and partially mapped crossover[32] was used to pass parts of uniformly randomly sampled length to the next generation. The best fitted patterns are passed on to the next generation through sample-wise (tournament) selection. In this fashion, a population will converge to local optimality. To improve convergence and approach global optimality, an island-model approach was used[33]; the algorithm runs on multiple randomly initialized populations (islands) in parallel, which explore the solution space independently without a priori partitioning. Information between populations is exchanged through migration. Critical algorithm parameters are (1) the population size on each island, (2) the mutation probability, (3) the crossover probability, (4) the number of islands, (5) the migration interval, and (6) the migration size (see Supplementary Material - GA configuration and fine-tune). These parameters were optimized through testing and benchmarking on one patient. As calculation times depend strongly on target volume, a case with a relatively small target (PTV = 8.2 cc) was used to enable rapid prototyping (see Supplementary Material - Computational requirements and convergence). The final configuration of the GA consisted of a population of 50 times the number of pencil beams, evenly distributed over 20 islands. The crossover and mutation probabilities were respectively 0.8 and 0.1 for each individual. The initial configuration of all individuals was selected as the best fitting from a randomly generated set of 10 times the population (ie, 500 times the number of pencil beams). After selection and for every 15 generations, 5% of the population of each island was migrated. Convergence was defined by no further improvement for 25 consecutive generations on all islands. More details on the configuration of the algorithm are described in the Supplementary Material.

Results

Optimized scan patterns

Typical examples of the standard (nonoptimized) line-by-line and optimized scan patterns and the resulting PBS-DR distributions in a transverse plane through the PTV are shown in Figure 3. The corresponding PBS-DR distributions are shown as colored overlays in the plots, with the PTV and GTV contours. PTV volumes range from 8.2 cc to 83.9 cc. For small PTVs, the optimized patterns combine a circular closed loop with radial inward and outward displacements around the central region. The highest PBS-DR is realized in a ring surrounding the GTV. For larger patterns, the closed loop wraps around itself in a swirl. The corresponding PBS-DR distributions have a C shape for the smaller patterns and a swirl-like shape for the larger ones. As all pencil beams must be delivered, it is unavoidable that the FLASH-compatible PBS-DR is reduced at some positions, which for the optimized patterns corresponds to the central region near both the initial and final positions. The pencil-beam distribution is the same for the optimized patterns and the standard line-by-line due to the sequential

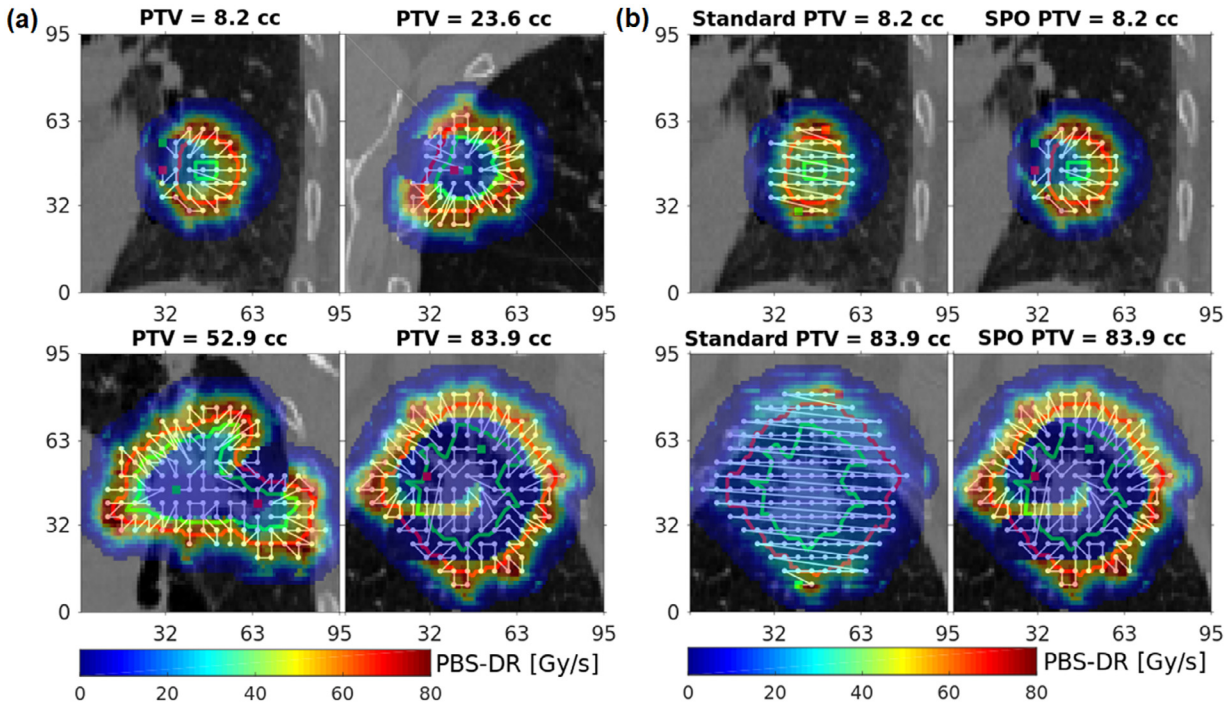

Fig. 3. (a) optimized scan patterns and (b) comparison of standard (nonoptimized) line-by-line and optimized scan patterns with initial (green) and final (red) positions and, color-coded in the background, the resulting pencil-beam scanning-dose rate distribution in a beam transverse plane through the gross tumor volume (green) and the planning target volume (red), translucently delineated.

application of the pattern optimizer, which only changes the order the same set of pencil beams is delivered.

The corresponding patient-population PBS-DR volume histograms for the optimized and the standard line-by-line patterns are shown in Figure 4. The dose rate is significantly higher for the optimized patterns, with the improvement over the standard line-by-line pattern being maximum for the considered FLASH dose-rate threshold.

Optimized FLASH coverage and PBS-DR

The optimized FLASH coverage of ipsilateral lung for all treatment beams and all treatment plans is shown as a function of the PTV volume in Figure 5. For small PTVs, fast irradiation times and, therefore, high PBS-DRs and large FLASH coverage are also achieved with the nonoptimized standard patterns. The optimizer opens the FLASH window for much larger PTVs up to 83.9 cc, with the

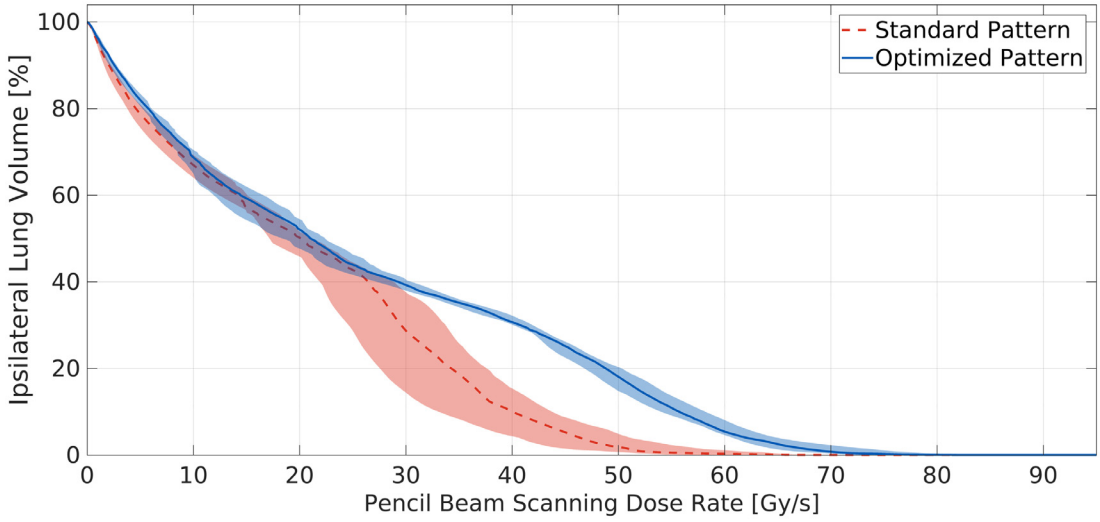

Fig. 4. Patient population median and the first and third quartiles of pencil-beam scanning-dose rate volume histograms for the ipsilateral lung with standard and optimized scan patterns.

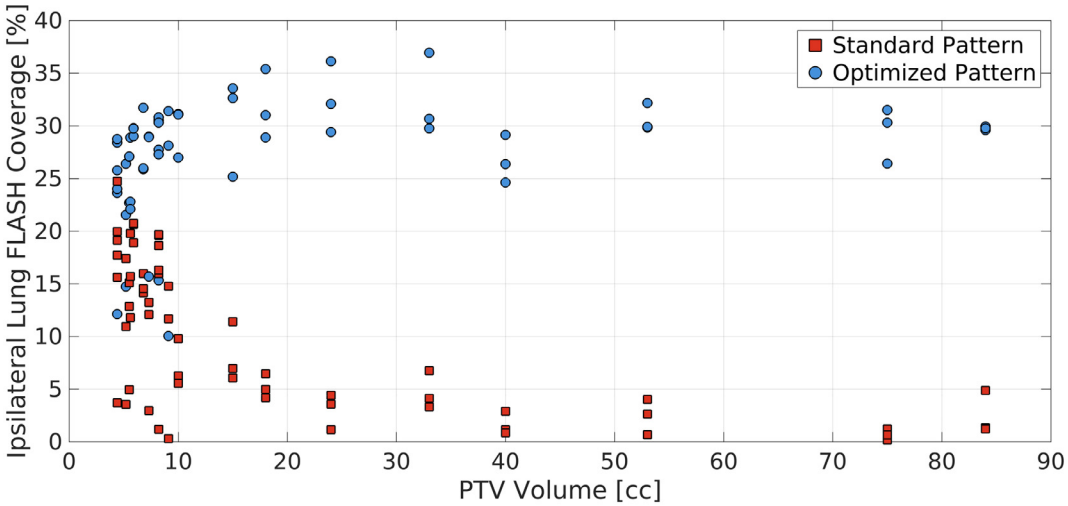

Fig. 5. The optimized FLASH coverage of ipsilateral lung for all treatment beams as a function of planning target volume volume. The FLASH coverage is defined as the volume fraction irradiated within FLASH conditions of >8 Gy and >40 Gy/s.

overall highest FLASH coverage for a PTV of 33.0 cc. An overall median FLASH coverage of 29.0% (full range, 10.0%-37.0%) and 6.9% (full range, 0.2%-24.7%) is obtained for the optimized and standard patterns, respectively, with an interquartile range of 4.7%-point and 12.4%-point, respectively. The median variation in FLASH coverage between the 3 beams for each plan was 2.5% (full range, 0.1%-21.0%) for the nonoptimized and 4.0% (full range, 0.0%-21.4%) for the optimized plans, respectively. The difference between the FLASH coverage of the best and the worst-performing patterns out of the various optimization runs was small, with a median of 0.7%-point (full range, 0%-8.7%-point).

The running time of the scan-pattern optimizer increased as the target volume increases. Median running times for a single run of 9 minutes, 54 minutes, and 133 minutes were obtained for groups of increasing target volume (0-20 cc, 20-40 cc, 40-80 cc), with median pencil-beam numbers of 36, 85, and 131, respectively.

The dependence on beam current of the FLASH coverage of the ipsilateral lung excluding the GTV is shown in Figure 6 for currents around the value used for the optimization (40 nA). The lines display the patient population median while the shadowed regions indicate the interquartile range. The optimized patterns lead to a consistently higher FLASH coverage and less interfraction/beam and interpatient variation than the standard pattern, already at low beam currents. At intermediate current values, the optimized patterns are robust against beam-current variations. For a variation of 5 nA around the values used for optimization (40 nA), FLASH coverage increases by 2.2%-point for higher beam current (45 nA) but decreases by 6.1%-point for the lower current (35 nA). At higher current values, the coverage is

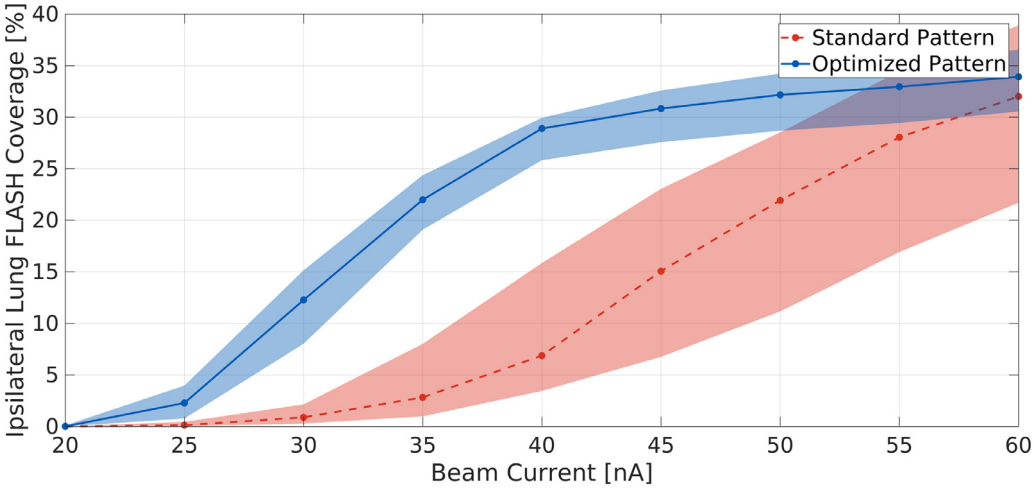

Fig. 6. Median, first, and third quartiles of the FLASH coverage in the ipsilateral lung, excluding the gross tumor volume, for standard and optimized scan patterns, optimal for 40 nA but evaluated on different beam currents.

similar for both patterns as global FLASH coverage is achieved.

Discussion

In this article, we have applied a GA to maximize the FLASH coverage in PT of small lung lesions through optimization of the pencil-beam scan pattern. The optimization was performed sequentially after pencil-beam selection and a multicriteria optimization of the physical dose distribution per beam. It has no effect on the nominal dose distribution. In optimizing the scan patterns, we have assumed that the delivery is combined with adequate breathing motion mitigation (eg, breath hold), so that the effect of that intrafraction variation and interplay effect on the delivered dose is negligible. Beam current fluctuations, however, may be critical as they lead to variations in the instantaneous dose rate. Still, the results in Figure 6 indicate that the FLASH window, as opened through the scan-pattern optimization, does not drastically change for slightly different beam currents.

SPO is based on the PBS-DR[22] as a FLASH metric. Due to the threshold value of 1 cGy, the PBS-DR is quasilocal in that, for a given voxel, it only depends on the delivery of nearby pencil beams. We chose the beam current and machine parameters such that the FLASH effect cannot be achieved globally. Too high beam currents compromise plan quality terms of physical dose due a minimal pencil-beam delivery time, requiring further pencil-beam reduction, and optimized beam currents for each beam and each plan may not be technologically feasible in routine clinical practice. In calculating the PBS-DR, we neglected pencil-beam switching times. They are small in comparison to the delivery times and depend on the details of the pencil-beam scanning setup. More accurate modeling is necessary for clinical evaluation of the PBS-DR. With a full range of estimated pencil-beam delivery times of 0.002 to 66.8 ms a fast-monitoring system is necessary for delivery of these plans. With only 1.6% below 1 ms, there may also be room for further pencil-beam reduction. With a beam current larger than the 40 nA used here, through SPO local FLASH conditions and partial FLASH coverage come within reach for treatment of larger targets. The optimized patterns reflect this quasilocal nature and prioritize the consecutive delivery of nearby pencil beams in the transverse plane, particularly in the high-dose volume surrounding the target. With increasing target volume, the patterns develop a swirl-like shape to still achieve FLASH condition in as much of healthy-tissue volume as possible. As all pencil beams must be delivered, the PBS-DR and, therefore, the FLASH effect is necessarily compromised in some voxels. For the optimized patterns, the initial and final positions are placed in the center as pencil beam overlap, compromising the PBS-DR, is unavoidable there and gains can be achieved only in the outer regions. The smallest target volumes (below 10 cc) are different in this regard. The center and outward regions are covered by the same pencil beams and the initial and final positions are placed on the edge of the pattern. Due to the smaller number of pencil beams and the bigger relative effect of the irregular target shape, also a larger variation in FLASH coverage is observed for the smaller targets, both between treatment beams and patients (Fig. 5).

Although the configuration of the GA was primarily done using a single case with relatively modest PTV of 8.2 cc, the SPO gives consistent results over a wide range of PTVs and adds new features for the largest volumes. This may, in part, be due to the fact that this is a very homogeneous patient group. The optimization implemented here puts equal weight on all nontarget healthy tissue irradiated to >8 Gy. Different priorities could be given to different healthy tissue volumes and further improvement could be achieved through an integrated simultaneous optimization of dose and dose rate, respectively, through lateral pencil beam position and weights and through the scan pattern, also addressing breathing motion and other treatment uncertainties. Balancing the trade-off between dose and dose rate in such an optimization, however, would also need more insight in the mechanisms of FLASH. We aimed at maximizing the FLASH coverage, defined as the healthy-tissue volume percentage that is irradiated within strict FLASH conditions (ie, [fraction] dose >8 Gy and PBS-DR >40 Gy/s). This is a geometric FLASH metric.

The biological and physiological mechanisms underlying the FLASH effect are not fully unraveled yet. The assumptions made here are in line with on what is currently known. Based on future insights on the effect of delivery dynamics in FLASH-PT with PBS, the GA could be further optimized and fine-tuned. It could be extended to a dosimetric metric through dose-weighting of voxel doses or more advanced modeling of the FLASH effect to minimize the FLASH-enhanced mean lung dose (see Supplementary Material - Results on FLASH-enhanced dose) or the volume receiving FLASH-enhanced and nonenhanced dose contributions adding up to 20 Gy equivalent dose.

A fundamental limitation of GAs is their stochastic nature. Furthermore, a patient with a relatively small target was used to optimize the configuration of the GA, which, therefore, may not be absolutely optimal for larger targets. Extensive validation on the patient cohort studied here, however, has shown that, although the optimized scan patterns differ between different runs of the algorithm and the configuration may not be optimal for all cases, the resulting variations in the distribution of PBS-DR and FLASH coverage are very small. In fact, they are much smaller than interpatient variation and differences between treatment beams for one patient. Nonetheless, further fine-tuning and validation may be required for different applications and treatment sites.

Current FLASH proton therapy is limited to the highest cyclotron energy of 250 MeV. Both conventional passive scattering and Bragg-peak IMPT with an energy degrader and energy-selection system compromise the instantaneous dose rate well below the FLASH threshold. FLASH-compatible beam hardware, in particular 3-dimensonal printed ridge filters,[34] which may instantaneously convert a 250 MeV

pristine pencil beam into a lower energy spread-out Bragg-peak, have been developed.[35-38] As conventional lateral scattering to irradiate larger target volumes still compromises the dose rate, these may be also combined with pencil-beam scanning. In this context, scan pattern optimization may also lead to significantly higher PBS-DRs.

We focused on single-beam per fraction treatments to 54 Gy in 3 fractions. This comes at the expense of healthy tissue sparing through fractionation.[28] Moreover, beam doses of 18 Gy may lead to high dose near the entrance and exit of the beams. Depending on the strength of the FLASH effect this may or may not be clinically acceptable and treatments with more beams and fractions may be desirable. SPO does not depend on the beam dose per se, and it could also be applied to more fractionated treatments.

Conclusion

We have shown that sequential scan-pattern optimization in stereotactic PT with transmission beams of small lung lesions leads to a significant increase in PBS-DR and, therefore, potentially to better healthy-tissue sparing through FLASH. In particular for patients with limited lung function (eg, due to underlying lung disease or for treatment of multiple metastatic lesions), this may be relevant. The configuration of the GA used to optimize the pattern is flexible and may be further fine-tuned or optimized, based on the exact conditions under which the FLASH effect occurs. More research on the effect of the time structure in the delivery of IMPT with PBS on FLASH and the exact dose and dose-rate thresholds is essential.

References

1. Favaudon V, Caplier L, Monceau V, et al. Ultrahigh dose-rate FLASH irradiation increases the differential response between normal and tumor tissue in mice. *Sci Transl Med* 2014;6:245ra93.
2. Dewey DL, Boag JW. Modification of the oxygen effect when bacteria are given large pulses of radiation. *Nature* 1959;183:1450–1451.
3. Hornsey S, Alper T. Unexpected dose-rate effect in the killing of mice by radiation. *Nature* 1966;210:212–213.
4. Favaudon V, Labarbe R, Limoli CL. Model studies of the role of oxygen in the FLASH effect. *Med Phys* 2022;49:2068–2081.
5. Friedl AA, Prise KM, Butterworth KT, Montay-Gruel P, Favaudon V. Radiobiology of the FLASH effect. *Med Phys* 2021;49:1–21.
6. Montay-Gruel P, Petersson K, Jaccard M, et al. Irradiation in a FLASH: Unique sparing of memory in mice after whole brain irradiation with dose rates above 100Gy/s. *Radiother Oncol* 2017;124:365–369.
7. Vozenin MC, De Fornel P, Petersson K, et al. The advantage of FLASH radiotherapy confirmed in mini-pig and cat-cancer patients. *Clin Cancer Res* 2019;25:35–42.
8. Bourhis J, Sozzi WJ, Jorge PG, et al. Treatment of a first patient with FLASH-radiotherapy. *Radiother Oncol* 2019;139:18–22.
9. Zlobinskaya O, Siebenwirth C, Greubel C, et al. The effects of ultrahigh dose rate proton irradiation on growth delay in the treatment of human tumor xenografts in nude mice. *Radiat Res* 2014;181:177–183.
10. Beyreuther E, Brand M, Hans S, et al. Feasibility of proton FLASH effect tested by zebrafish embryo irradiation. *Radiother Oncol* 2019;139:46–50.
11. Girdhani S, Abel E, Katsis A, et al. FLASH: A novel paradigm changing tumor irradiation platform that enhances therapeutic ratio by reducing normal tissue toxicity and activating immune pathways [Abstract]. In: *Proceedings of the American Association for Cancer Research Annual Meeting 2019; Atlanta, GA*. 79, Philadelphia, USA: AACR; 2019:LB–280. Cancer Res.
12. Diffenderfer ES, Verginadis II, Kim MM, et al. Design, implementation, and in vivo validation of a novel proton FLASH radiation therapy system. *Int J Radiat Oncol Biol Phys* 2020;106:440–448.
13. Velalopoulou A, Karagounis IV, Cramer GM, et al. FLASH proton radiotherapy spares normal epithelial and mesenchymal tissues while preserving sarcoma response. *Cancer Res* 2021;81:4808–4821.
14. Cunningham S, McCauley S, Vairamani K, et al. FLASH proton pencil beam scanning irradiation minimizes radiation-induced leg contracture and skin toxicity in mice. *Cancers* 2021;13:1012.
15. Breneman J. Feasibility Study of FLASH Radiotherapy for the Treatment of Symptomatic Bone Metastases (FAST-01) 2020, March; Identifier NCT04592887. Available at: https://clinicaltrials.gov/ct2/show/study/NCT04592887. Accessed January 24, 2022.
16. Mou B, Beltran CJ, Park SS, Olivier KR, Furutani KM. Feasibility of proton transmission-beam stereotactic ablative radiotherapy versus photon stereotactic ablative radiotherapy for lung tumors: A dosimetric and feasibility study. *PloS One* 2014;9:e98621.
17. van Marlen P, Dahele M, Folkerts MM, Slotman BJ, Verbakel WFAR. Conventionally fractionated FLASH treatment planning for head and neck cancer using transmission beam proton therapy. *Int J Radiat Oncol Biol Phys* 2020;108:S186–S187.
18. van Marlen P, Dahele M, Folkerts M, Abel E, Slotman BJ, Verbakel W. Ultra-high dose rate transmission beam proton therapy for conventionally fractionated head and neck cancer: Treatment planning and dose rate distributions. *Cancers* 2021;13:1859.
19. van de Water S, Safai S, Schippers JM, Weber DC, Lomax AJ. Towards FLASH proton therapy: The impact of treatment planning and machine characteristics on achievable dose rates. *Acta Oncologica* 2019;58:1463–1469.
20. Gao H, Lin B, Lin Y, et al. Simultaneous dose and dose rate optimization (SDDRO) for FLASH proton therapy. *Med Phys* 2020;47:6388–6395.
21. Lin Y, Lin B, Fu S, et al. SDDRO-joint: Simultaneous dose and dose rate optimization with the joint use of transmission beams and Bragg peaks for FLASH proton therapy. *Phys Med Biol* 2021;66: 125011.
22. Folkerts MM, Abel E, Busold S, et al. A framework for defining FLASH dose rate for pencil beam scanning. *Med Phys* 2020;47:6396–6404.
23. Breedveld S, Storchi PRM, Voet PWJ, Heijmen BJM. iCycle, Integrated, multicriterial beam angle, and profile optimization for generation of coplanar and noncoplanar IMRT plans. *Medical Physics* 2012;39:951–963.
24. Kooy HM, Clasie BM, Lu HM, et al. A case study in proton pencil-beam scanning delivery. *Int J Radiat Oncol Biol Phys* 2010;76:624–630.
25. Kouwenberg J, Penninkhof J, Habraken S, Zindler J, Hoogeman M, Heijmen B. Model based patient pre-selection for intensity-modulated proton therapy (IMPT) using automated treatment planning and machine learning. *Radiotherapy and Oncology* 2021;158:224–229.
26. Timmerman R, Paulus R, Galvin J, et al. Stereotactic body radiation therapy for inoperable early stage lung cancer. *JAMA* 2010;303:1070–1076.
27. van de Water S, Kraan AC, Breedveld S, et al. Improved efficiency of multi-criteria IMPT treatment planning using iterative resampling of randomly placed pencil beams. *Physics in Medicine and Biology* 2013;58:6969–6983.
28. Habraken S, Breedveld S, Groen J, Nuyttens J, Hoogeman M. Trade-off in healthy tissue sparing of FLASH and fractionation in stereotactic proton therapy of lung lesions with transmission beams. *Radiotherapy and Oncology* 2022.
29. Larrañaga P, Kuijpers CMH, Murga RH, Inza I, Dizdarevic S. Genetic algorithms for the travelling salesman problem: A review of representations and operators. *Artificial Intelligence Review* 1999;13:129–170.

30. Bhatt N, Chauhan NR. Genetic algorithm applications on Job Shop Scheduling Problem: A review. 2015 International Conference on Soft Computing Techniques and Implementations. New York, USA: IEEE; 2015:7–14.
31. Virgolin M, De Lorenzo A, Medvet E, Randone F. Learning a formula of interpretability to learn interpretable formulas. In: Thomas Bäck T, Preuss N, Deutz A, Wang H, Doerr C, Emmerich M, Trautmann H, eds. *Parallel Problem Solving from Nature – PPSN XVI*. New York, USA: Springer; 2020:79–93.
32. Goldberg DE, Lingle R. Alleles, loci, and the traveling salesman problem. In: Grefenstette JJ, ed. *Proceedings of 1st International Conference on Genetic Algorithms*. 154, Pittsburgh, USA: Carnegie-Mellon University; 1985:154–159.
33. Whitley D, Rana S, Heckendorn RB. The island model genetic algorithm: On separability, population size and convergence. *J Comput Inf Sci Eng* 1998;7:32–47.
34. Simeonov Y, Weber U, Penchev P, et al. 3D range-modulator for scanned particle therapy: Development, Monte Carlo simulations and experimental evaluation. *Phys Med Biol* 2017;62:7075.
35. Patriarca A, Fouillade C, Auger M, et al. Experimental set-up for FLASH proton irradiation of small animals using a clinical system. *Int J Radiat Oncol Biol Phys* 2018;102:619–626.
36. Darafsheh A, Hao Y, Zwart T, et al. Feasibility of proton FLASH irradiation using a synchrocyclotron for preclinical studies. *Med Phys* 2020;47:4348–4355.
37. Evans T, Cooley J, Wagner M, Yu T, Zwart T. Demonstration of the FLASH effect within the spread-out Bragg peak after abdominal irradiation of mice. *Int J Part Ther* 2022;8:68–75.
38. Kim MM, Verginadis II, Goia D, et al. Comparison of FLASH proton entrance and the spread-out Bragg peak dose regions in the sparing of mouse intestinal crypts and in a pancreatic tumor model. *Cancers (Basel)* 2021;13:4244.